
Figures and figure supplements

DCC regulates astroglial development essential for telencephalic morphogenesis and corpus callosum formation

Laura Morcom et al

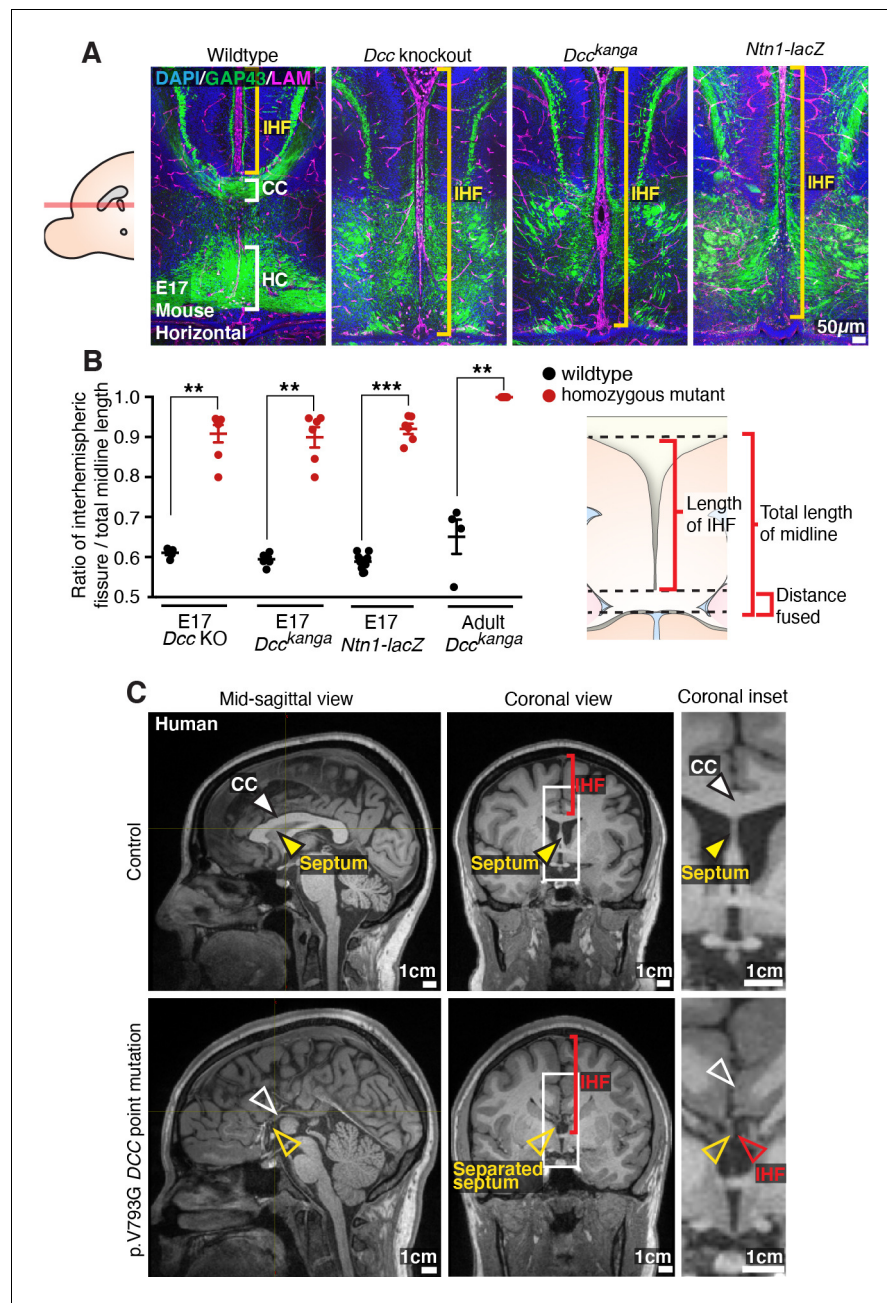


Figure 1. Netrin 1 (NTN1) and deleted in colorectal carcinoma (DCC) are crucial for remodelling of the interhemispheric fissure (IHF), corpus callosum (CC) and hippocampal commissure (HC) formation. (A) Staining for Gap43-positive axons (green) and pan-Laminin (LAM)-positive leptomeninges and basement membrane (magenta) in wildtype, *Dcc* knockout, *Dcc^{kanga}*, and *Ntn1-lacZ* mice at embryonic day (E)17 indicates midline formation or absence of the CC and HC (white brackets) and extent of the IHF (yellow brackets). (B) The ratio of IHF length over the total midline length with schema. (C) T1-weighted MR images of a control subject compared with an individual with a DCC mutation demonstrate the presence or absence of the CC (white arrowheads) and extent of the IHF (red arrowheads and brackets) within the septum (yellow arrowheads). Graph represents mean \pm SEM. Statistics by Mann-Whitney test: ** $p < 0.01$, *** $p < 0.001$. See related **Figure 1—figure supplement 1** and **Supplementary file 1**.

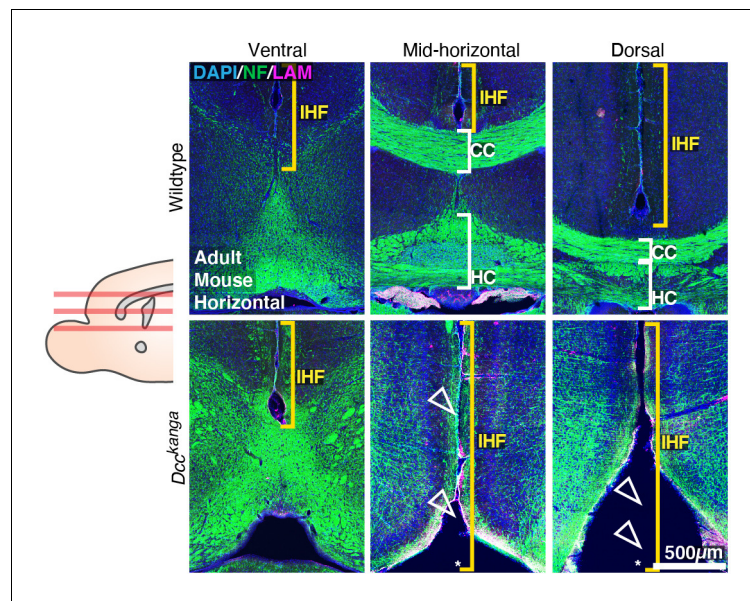


Figure 1—figure supplement 1. The interhemispheric fissure (IHF) is not remodelled in adult *Dcc^{kanga}* mice. Neurofilament (NF)-positive axons (green) and pan-Laminin (LAM)-positive leptomeninges and basement membrane (magenta) in adult wildtype and *Dcc^{kanga}* mice reveal presence/absence of the corpus callosum (CC) and hippocampal commissure (HC) (white brackets and arrowheads), the extent of the interhemispheric fissure (IHF) (yellow brackets) and absence of the septal substrate in *Dcc^{kanga}* mice (asterisks).

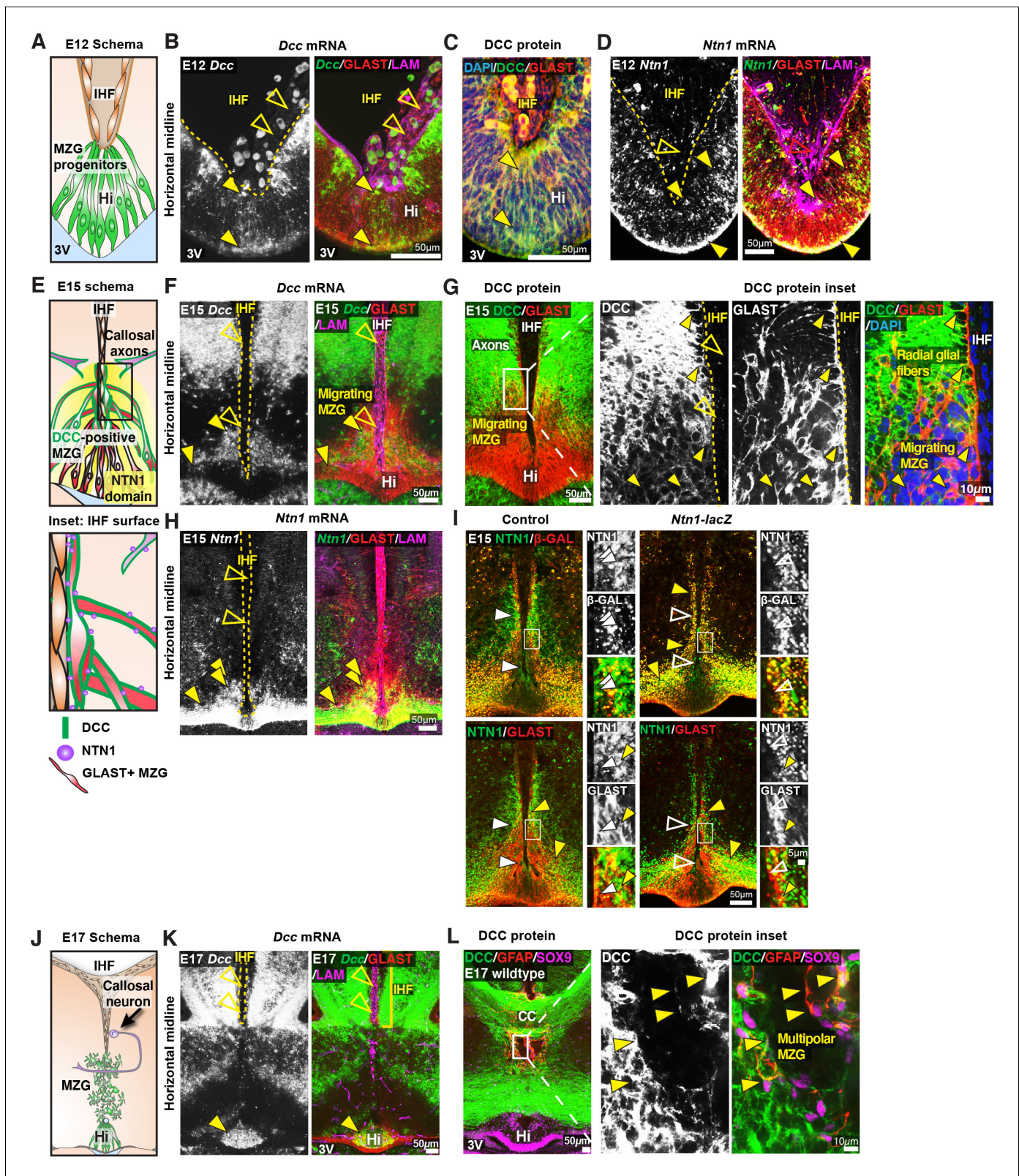


Figure 2. Deleted in colorectal carcinoma (DCC) and netrin 1 (NTN1) are expressed in midline zipper glia (MZG) and MZG progenitors. (A, E, J) Schematics depicting the cellular composition of the ventral telencephalic midline at embryonic day (E)12, E15 and E17. (B, F, K) *Dcc* mRNA (green), Glast-positive glia (red) and pan-Laminin (LAM)-positive leptomeninges and basement membrane (magenta) in E12, E15 and E17 wildtype mice reveal *Dcc*-positive/Glast-positive glial fibres (yellow arrowheads) and absence of *Dcc* within the interhemispheric fissure (IHF) (open yellow arrowheads). (C, G) Figure 2 continued on next page

Figure 2 continued

DCC protein (green) and Glial protein (red) at E12 and E15 in wildtype mice reveal DCC-positive/Glial-positive glial fibres (yellow arrowheads) and absence of DCC within the IHF (open yellow arrowheads). (D, H) *Ntn1* mRNA (green), Glial (red) and pan-LAM (magenta) in E12 and E15 wildtype mice show *Ntn1*-positive/Glial-positive glial fibres (yellow arrowheads) and absence of *Ntn1* within the IHF (open yellow arrowheads). (E, inset) Schema of DCC and NTN1 expression at the E15 IHF surface, based on the results from F–I and **Figure 2—figure supplement 1**. (I) NTN1 (green) and Glial (red) or β -galactosidase (β -GAL; red) immunolabelling in E15 control and *Ntn1-lacZ* mice identify regions of NTN1 staining present in control heterozygotes and absent in homozygous *Ntn1-lacZ* mice (white arrowheads) and NTN1-/ β -GAL-positive puncta located in Glial-positive glia (yellow arrowheads), with insets. (L) DCC protein (green), glial-specific nuclear marker SOX9 (magenta) and mature astroglial marker (GFAP) in E17 wildtype mice identify DCC-positive/GFAP-positive/SOX9-positive glia (yellow arrowheads). 3V: third ventricle; Hi: telencephalic hinge. See related **Figure 2—figure supplement 1**.

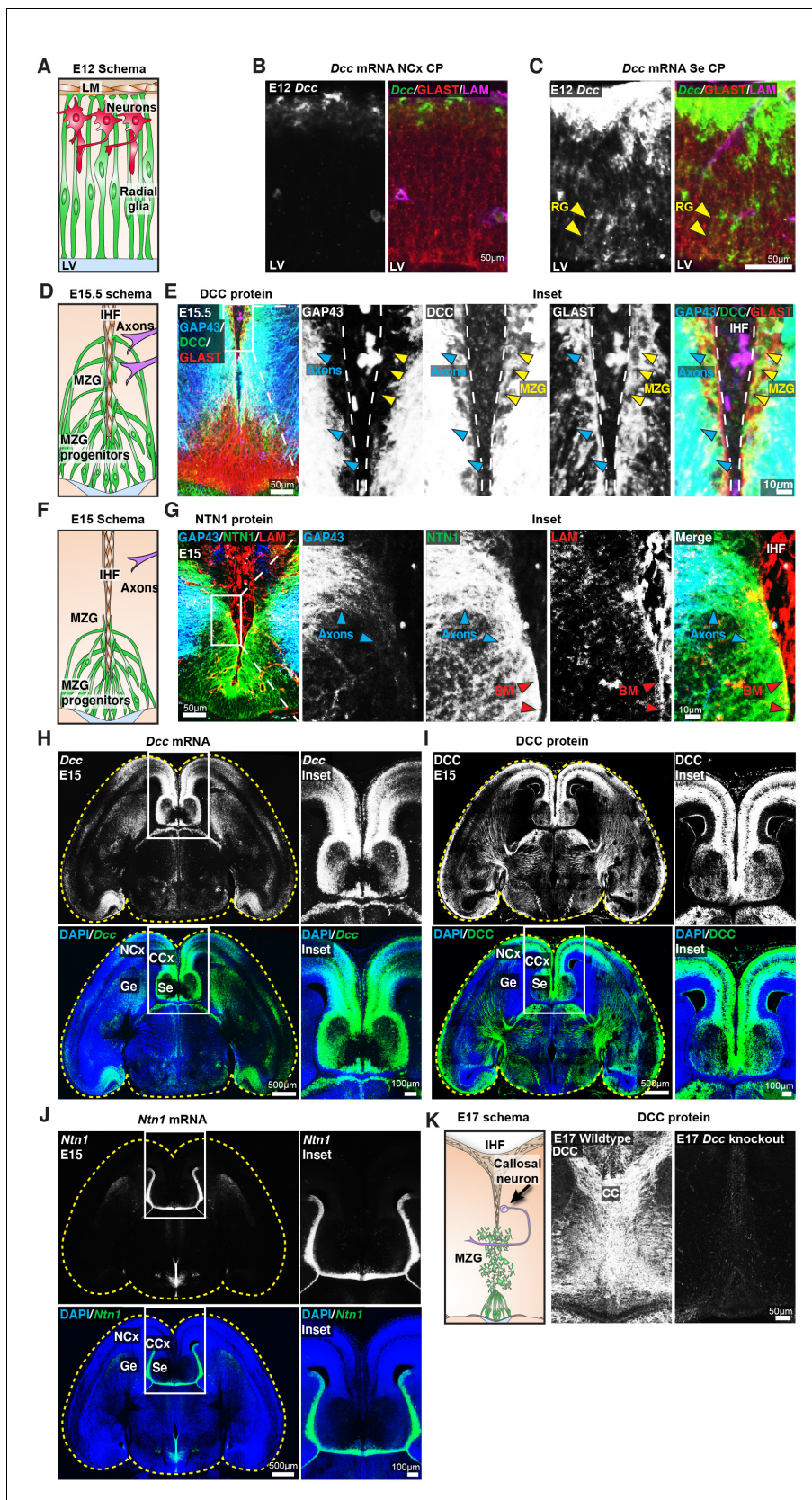


Figure 2—figure supplement 1. Deleted in colorectal carcinoma (DCC) is expressed in midline zipper glia (MZG). (A, D, F) Schemas of key cellular components within the telencephalic midline. (B, C) *Dcc* mRNA (green), Glast-positive glia (red) and pan-Laminin (LAM)-positive leptomeninges and Figure 2—figure supplement 1 continued on next page

Figure 2—figure supplement 1 continued

basement membrane (magenta) across the cortical plate (Cp) within the neocortex (NCx) or septum (Se) in horizontal sections of wildtype mice reveal *Dcc*-positive/Glast-positive radial glial (RG) fibres (yellow arrowheads). LV: lateral ventricle. (E) DCC protein (green), Gap43-positive axons (blue) and Glast-positive MZG (red) in horizontal sections of embryonic day (E)15 wildtype mice (right panels) indicate DCC-positive/Glast-positive cells (yellow arrowheads) and DCC-positive/Gap43-positive axons (blue arrowheads) that are approaching the midline and are adjacent to MZG. (G) Gap43-positive axons (blue), netrin 1 (NTN1) protein (green) and pan-LAM-positive leptomeninges and basement membrane (red) in horizontal sections of E15 wildtype mice reveal NTN1-positive/Gap43-positive axons (blue arrowheads) approaching the midline and NTN1-positive/LAM-positive basement membrane (BM; red arrowheads) of the interhemispheric fissure (IHF). (H–J) Mid-horizontal tissue sections encompassing the entire telencephalon (yellow outlines) with in situ hybridization for *Dcc* mRNA or *Ntn1* mRNA or immunohistochemistry for DCC protein (all white or green), counterstained with DAPI (blue). Insets of the telencephalic midline are shown on the right. (K) DCC immunohistochemistry in horizontal sections of E17 wildtype and *Dcc* knockout mice with schema of key cellular components within the telencephalic midline.

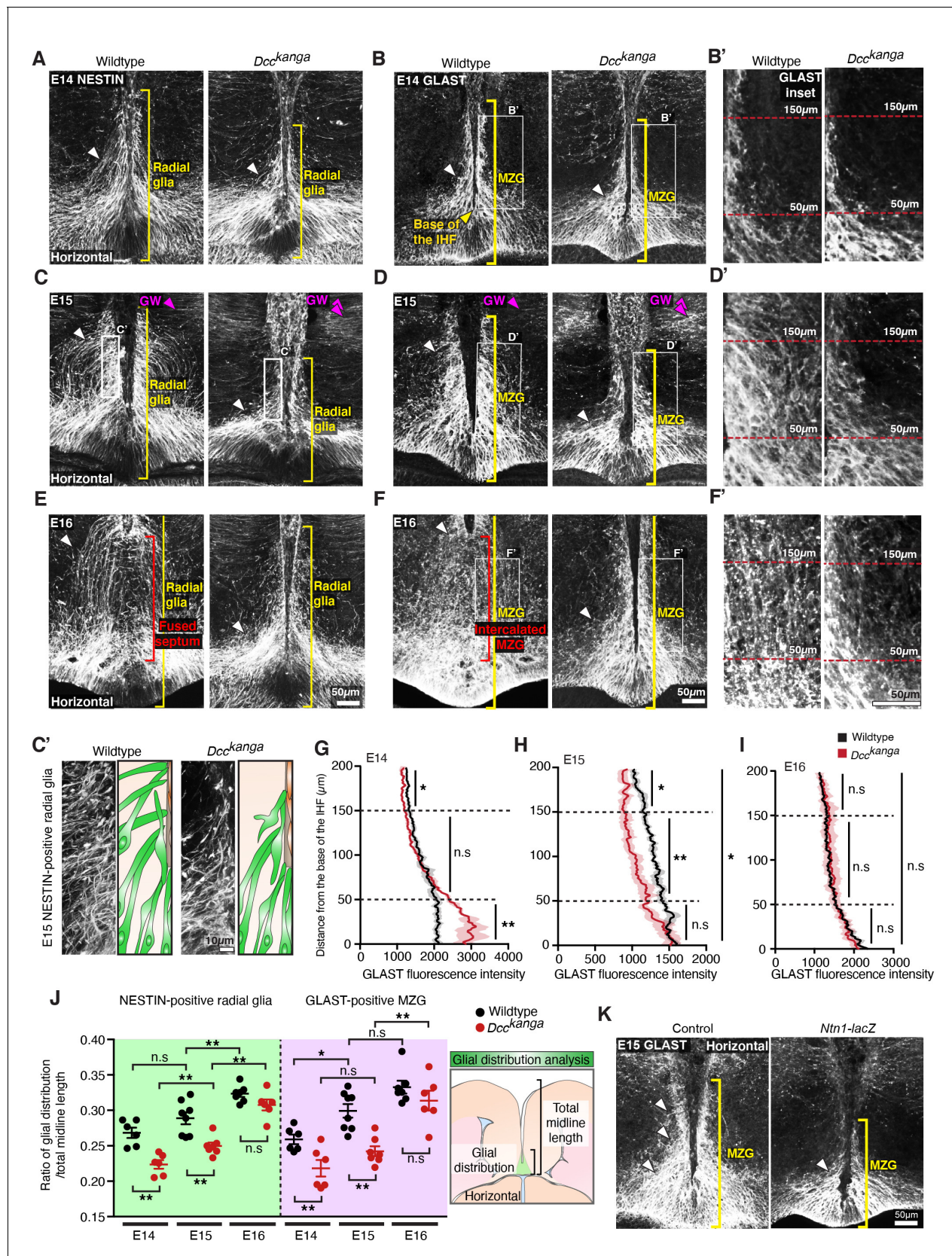


Figure 3. Netrin 1 (NTN1) and deleted in colorectal carcinoma (DCC) regulate midline zipper glia (MZG) morphology and spatial distribution. Nestin-positive radial glia (white; A, C, E) and Glial-positive glia (white; B, D, F, K) in embryonic day (E)14–E16 *Dcc^{kanga}* mice (A–F) and E15 *Ntn1-LacZ* mice (K) Figure 3 continued on next page

Figure 3 continued

demonstrate the distribution of glial processes along the interhemispheric fissure (IHF) surface (yellow brackets) and lateral to the IHF (white arrowheads) with insets (C', B', D', F'). Radial fibres of the glial wedge (GW) are indicated with magenta arrowheads. The mean fluorescence intensity of Glax staining between wildtype and *Dcc^{kanga}* mice at E14 (G), E15 (H) and E16 (I) based on the results from (B), (D) and (F), respectively. (J) The ratio of glial distribution over total midline length, with schema, based on the results from (A) to (F). All graphs represent mean \pm SEM. Statistics by Mann–Whitney test. n.s: not significant; * $p < 0.05$, ** $p < 0.01$. See related **Figure 3—figure supplement 1** and **Supplementary file 1**.

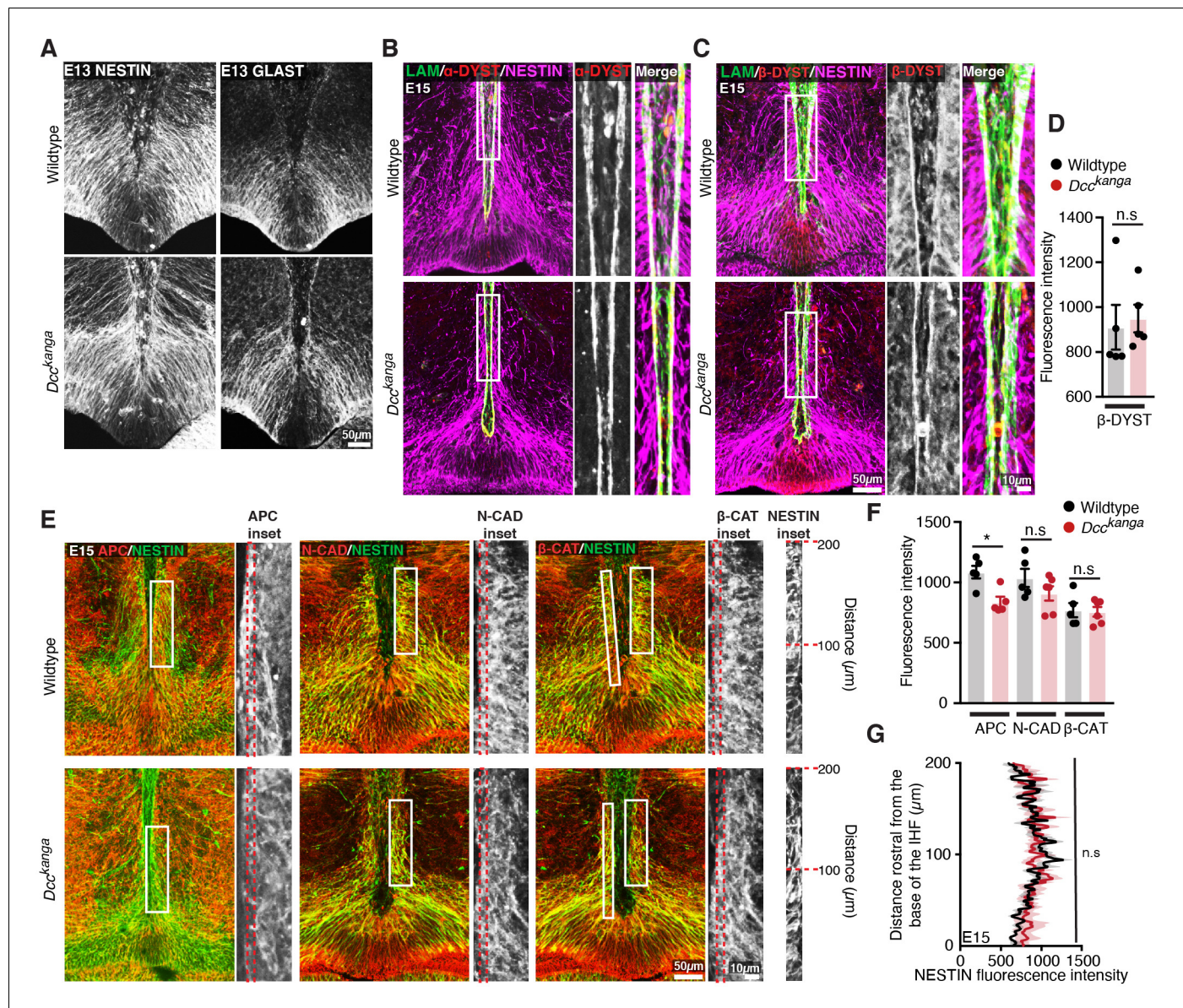
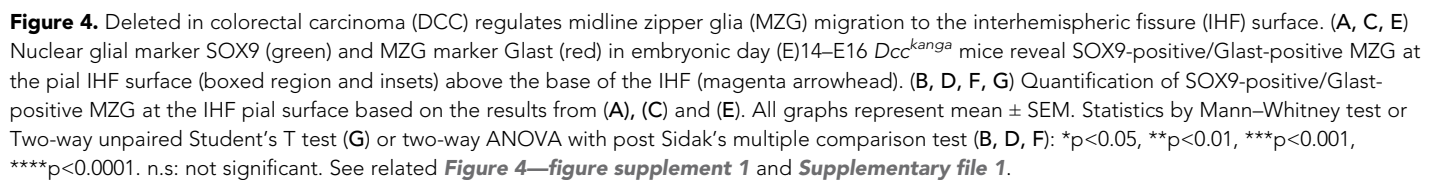


Figure 3—figure supplement 1. Deleted in colorectal carcinoma (DCC) is not required for endfeet attachment or molecular polarity of midline zipper glia (MZG). (A) Nestin-positive radial glia (white) and Glast-positive MZG (white) in horizontal sections of embryonic day (E)13 wildtype and *Dcc^{kanga}* mice. (B, C) Pan-Laminin (LAM)-positive leptomeninges and basement membrane (green), Nestin-positive radial glia (magenta) and α -dystroglycan (α -DYST; red; B) or β -dystroglycan (β -DYST; red, C) in horizontal sections of E15 wildtype and *Dcc^{kanga}* mice. (D) Quantification of fluorescence intensity of β -DYST along 200 μ m of the interhemispheric fissure (IHF) surface as outlined with red dotted box in (C). (E) Nestin-positive radial glia (green) with either adenomatous polyposis coli (APC, red), N-cadherin (N-CAD; red) or β -catenin (β -CAT; red) in horizontal sections of E15 wildtype and *Dcc^{kanga}* mice with insets. (F) Quantification of the fluorescence intensity of APC, N-CAD and β -CAT within 5 μ m of the IHF as outlined in red dotted-edged boxes from (E). (G) Quantification of the fluorescence intensity of Nestin-positive radial glial endfeet within 5 μ m of the IHF surface from inset in (E). All graphs represent mean \pm SEM. Statistics by Mann-Whitney test. n.s: not significant, * $p < 0.05$. See related **Supplementary file 1**.



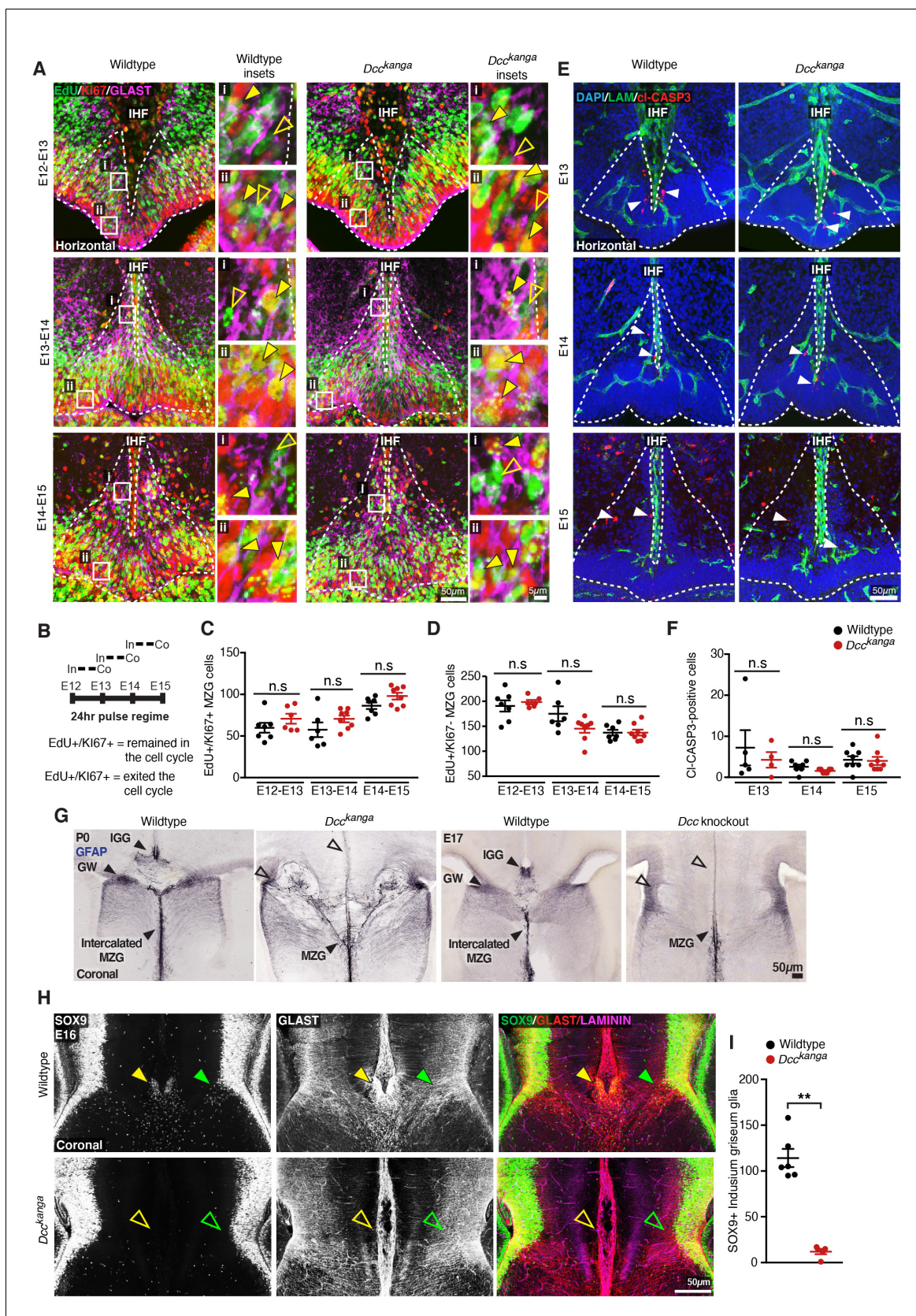


Figure 4—figure supplement 1. Deleted in colorectal carcinoma (DCC) does not regulate the proliferation or cell death of midline zipper glia (MZG) but regulates the formation of the indusium griseum glia and glial wedge. (A) Mouse MZG cells were birth-dated with the thymidine analog 5-ethynyl-*Figure 4—figure supplement 1 continued on next page*

Figure 4—figure supplement 1 continued

2'-deoxyuridine (EdU) every 24 hr, from embryonic day (E)12 to E15 in wildtype and *Dcc^{kanga}* mice. Representative images of EdU (green), cell cycle marker, Ki67 (red), and MZG marker Glast (magenta) are shown for wildtype and *Dcc^{kanga}* mice, with the distribution of MZG progenitors within the telencephalic hinge niche outlined with white dotted lines. Yellow arrowheads in insets point out EdU cells that are either Ki67-positive (filled arrowheads) or Ki67-negative (open arrowheads) in selected insets. The number of cells expressing each marker is quantified in (C) and (D). (B) Schema of the EdU injection (In) and collection (Co) regime and interpretation of co-labelled and non-co-labelled cells. (E) Laminin (LAM)-positive leptomeninges and basement membrane (green) and cleaved-caspase 3 (Cl-CASP3)-positive apoptotic cells (red, white arrowheads) in E13–E15 wildtype and *Dcc^{kanga}* mice. The number of Cl-CASP3-positive cells within the telencephalic hinge niche (white dotted lines) is quantified in (F). (G) Mature astroglial marker GFAP in coronal sections of P0 *Dcc^{kanga}* mice and E17 *Dcc* knockout mice and their wildtype littermates reveals midline glial populations, the glial wedge (GW), the indusium griseum glia (IGG) and the MZG (filled arrowheads) or their absence/malformation (open arrowheads). (H) Glial-specific cell body marker SOX9 (white or green), glial cell membrane marker Glast (white or red) and interhemispheric fissure (IHF) marker LAM (magenta) in E16 coronal sections from *Dcc^{kanga}* mice indicate the presence or absence of SOX9-positive/Glast-positive cell bodies at the pial surface of the IHF (yellow arrowheads) and within the intermediate zone (green arrowheads). (I) Quantification of SOX9-positive IGG cell bodies at the pial surface of the IHF in E16 wildtype and *Dcc^{kanga}* mice from immunohistochemistry in (G). All graphs represent mean \pm SEM. Statistics by Mann–Whitney test. n.s: not significant, ** $p < 0.01$. See related **Supplementary file 1**.

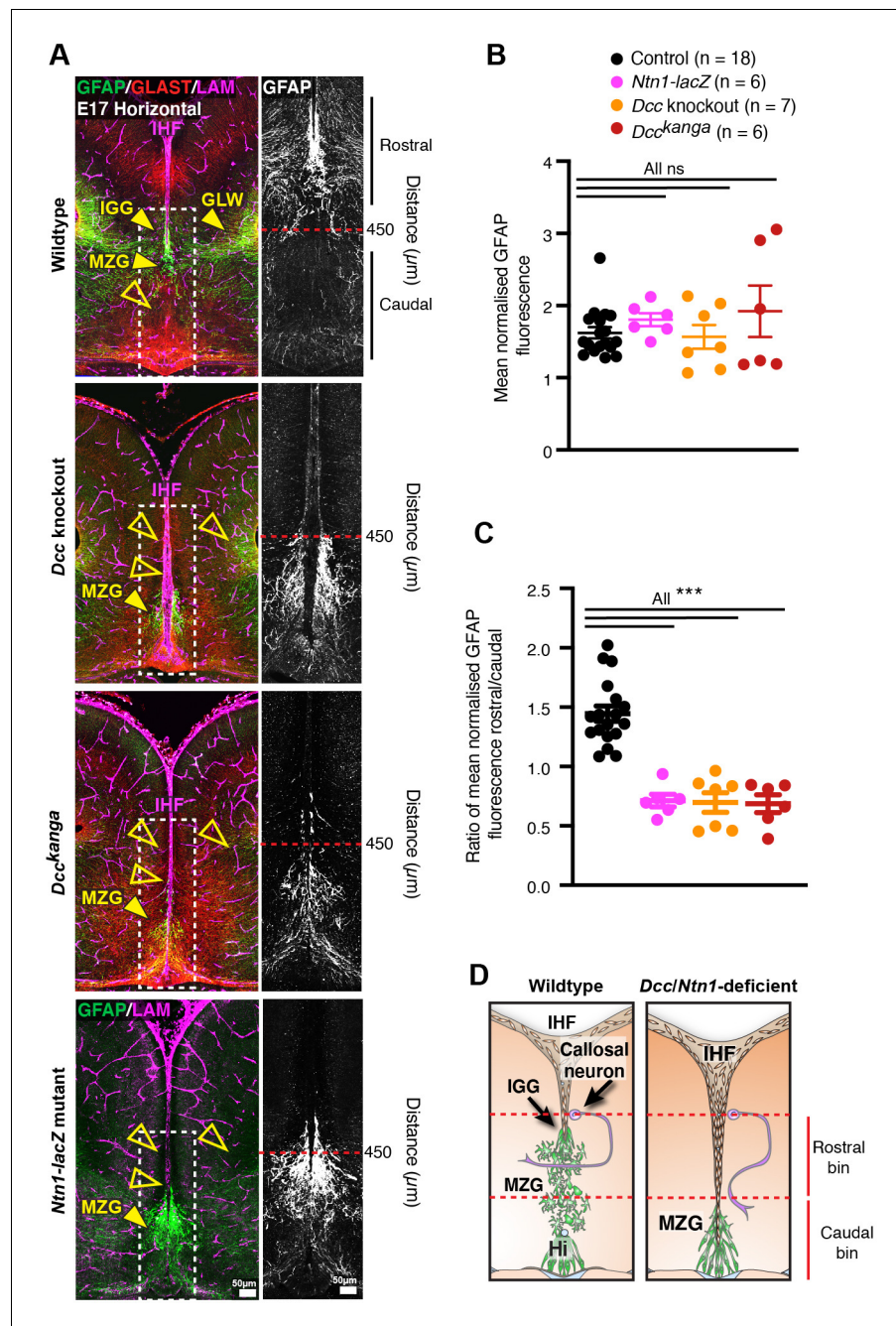


Figure 5. Netrin 1 (NTN1) and deleted in colorectal carcinoma (DCC) regulate midline zipper glia (MZG) organization during interhemispheric fissure (IHF) remodelling. (A) Gfap-positive mature astroglia (green or white in inset), Glast-positive glia (red) and pan-Laminin (LAM)-positive IHF and basement membrane (magenta) in embryonic day (E)17 wildtype *Dcc^{kanga}*, *Dcc* knockout and *Ntn1-LacZ* mice. Yellow arrowheads indicate presence (filled) or absence (open) of midline glial populations, the MZG, indusium griseum glia (IGG) and glial wedge (GW). Fluorescence intensity of Gfap staining from insets or bins in insets (red dotted line) was quantified in (B) and (C). (D) Schema of MZG development, IHF remodelling and corpus callosum (CC) formation in wildtype mice and mice deficient for NTN1 or DCC. Red dotted lines indicate rostral and caudal bins that were used to calculate the ratio of GFAP fluorescence in (C). All graphs represent mean ± SEM. Statistics by Kruskal–Wallis test with post-hoc Dunn’s multiple comparison test. *** $p < 0.001$; ns: not significant. See related **Figure 4—figure supplement 1**, **Figure 5—figure supplement 1** and **Supplementary file 1**.

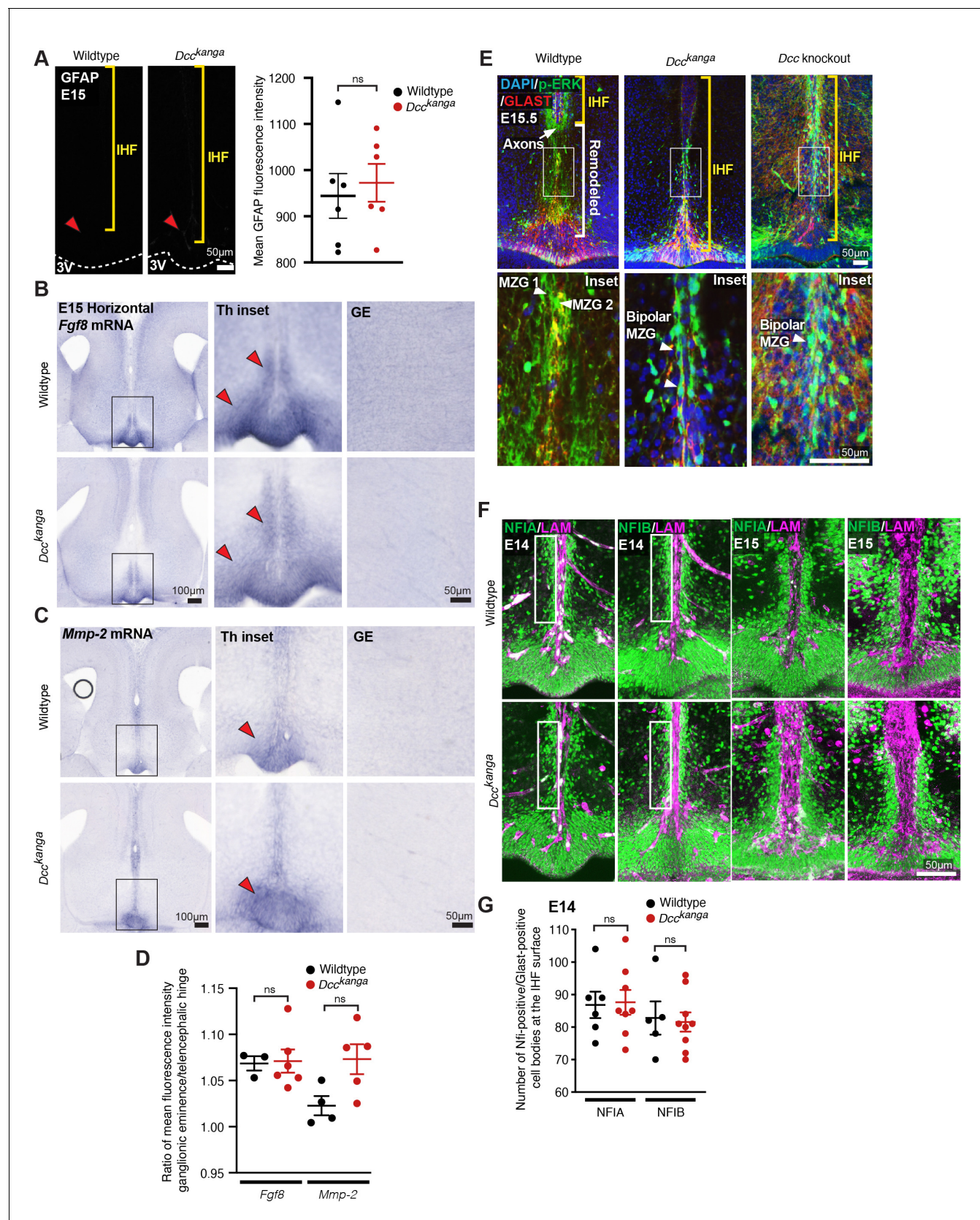


Figure 5—figure supplement 1. Deleted in colorectal carcinoma (DCC) is not required for astroglial differentiation of midline zipper glia (MZG). (A) Mature astroglial marker Gfap (white) in horizontal sections of embryonic day (E)15 wildtype and *Dcc^{kanga}* mice with quantification of Gfap average. Figure 5—figure supplement 1 continued on next page

Figure 5—figure supplement 1 continued

fluorescence intensity. The surface of the third ventricle (3V) is outlined with dotted white lines. Red arrowheads indicate reactive blood vessels that are not Gfap-positive glia. Yellow brackets indicate the position of the interhemispheric fissure (IHF). *Fgf8* mRNA (B) or *Mmp-2* mRNA (C) in horizontal sections of E15 wildtype and *Dcc^{kanga}* mice. Red arrowheads indicate reactivity in the telencephalic hinge (Th) in insets, right. A region of the ganglionic eminence (GE) where *Fgf8* is not expressed is shown and was used to normalize specific *Fgf8* expression within the Th with background immunoreactivity as quantified in (D). (E) Phosphorylated p44/42 Mapk or Erk1/2 (p-ERK, green) and Glast-positive MZG (red) in horizontal sections of E15.5 wildtype, *Dcc^{kanga}* mice and *Dcc* knockout mice reveal the extent of IHF (yellow brackets) and remodelled regions of the septum (white brackets) with p-ERK-positive MZG in insets. (F) Nuclear factor I (NFI) A or B (green) and pan-Laminin (LAM)-positive leptomeninges and basement membrane (magenta) in horizontal sections of E14 and E15 wildtype and *Dcc^{kanga}* mice. NFI-positive/Glast-positive MZG cell bodies at the IHF surface are outlined with white boxes and quantified in (G). Data is represented as mean \pm SEM. Significant differences were determined with nonparametric Mann–Whitney tests. ns: not significant.

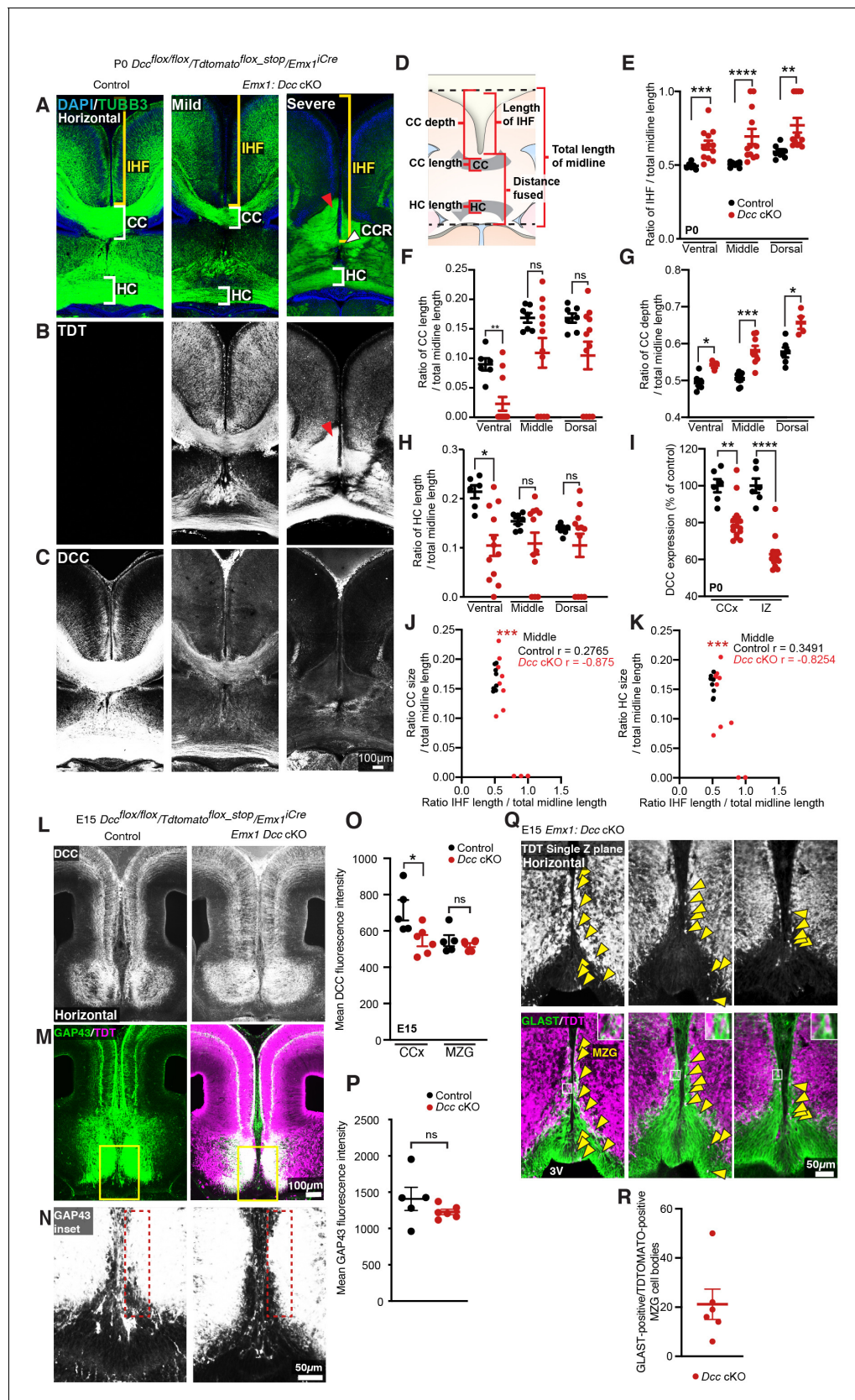


Figure 6. Conditional knockdown of deleted in colorectal carcinoma (DCC) within EMX1 cells causes a spectrum of callosal phenotypes. (A) Axonal marker TUBB3 (green), (B) TDT (white) or (C) DCC (white) in P0 *Dcc* cKO demonstrate a spectrum of callosal and interhemispheric fissure (IHF)

Figure 6 continued on next page

Figure 6 continued

remodelling phenotypes and a reduction in DCC expression within mice expressing *Emx1^{iCre}*. The corpus callosum (CC) or CC remnant (CCR) and hippocampal commissure (HC) are indicated with white brackets or white arrowheads, and the IHF is indicated with yellow brackets. Red arrowheads indicate axon bundles that have not crossed the midline. (D) Schema of measurements taken for quantification shown in (C–E). (E) Quantification of the ratio of IHF length normalized to total telencephalic midline length measured for P0 *Dcc* cKO mice. (F, G) Quantification of CC length (F) and depth (G) normalized to the total telencephalic midline length in P0 *Dcc* cKO mice. (H) Quantification of HC length normalized to the total telencephalic midline length in P0 *Dcc* cKO mice. (I) Quantification of DCC expression measured from the cingulate cortex (CCx) and intermediate zone (IZ) of *Dcc* cKO mice. (J, K) Scatterplots of the relationship between CC length (J) or HC length (K) normalized to total telencephalic midline length and IHF length normalized to total telencephalic midline length for middle horizontal sections of P0 *Dcc* cKO mice. Pearson *r* correlations are shown. (L) DCC (white), (M, N) axonal marker GAP43 (green or white, insets) and TDT (magenta) in embryonic day (E)15 *Dcc* cKO mice, with quantification of mean DCC fluorescence in (O) and quantification of mean GAP43 fluorescence within 50 μ m from the IHF (dotted red lines) in (P). (Q) TDT (white or magenta) and glial marker GLAST (green) in E15 *Dcc* cKO with insets and yellow arrowheads indicating GLAST-positive/TDT-positive MZG, and quantified in (R). All graphs represent mean \pm SEM. Statistics by Mann–Whitney test or unpaired t-test: **p*<0.05, ***p*<0.01, ****p*<0.001, *****p*<0.0001; n.s.: not significant. See related **Figure 5—figure supplement 1** and **Supplementary file 1**.

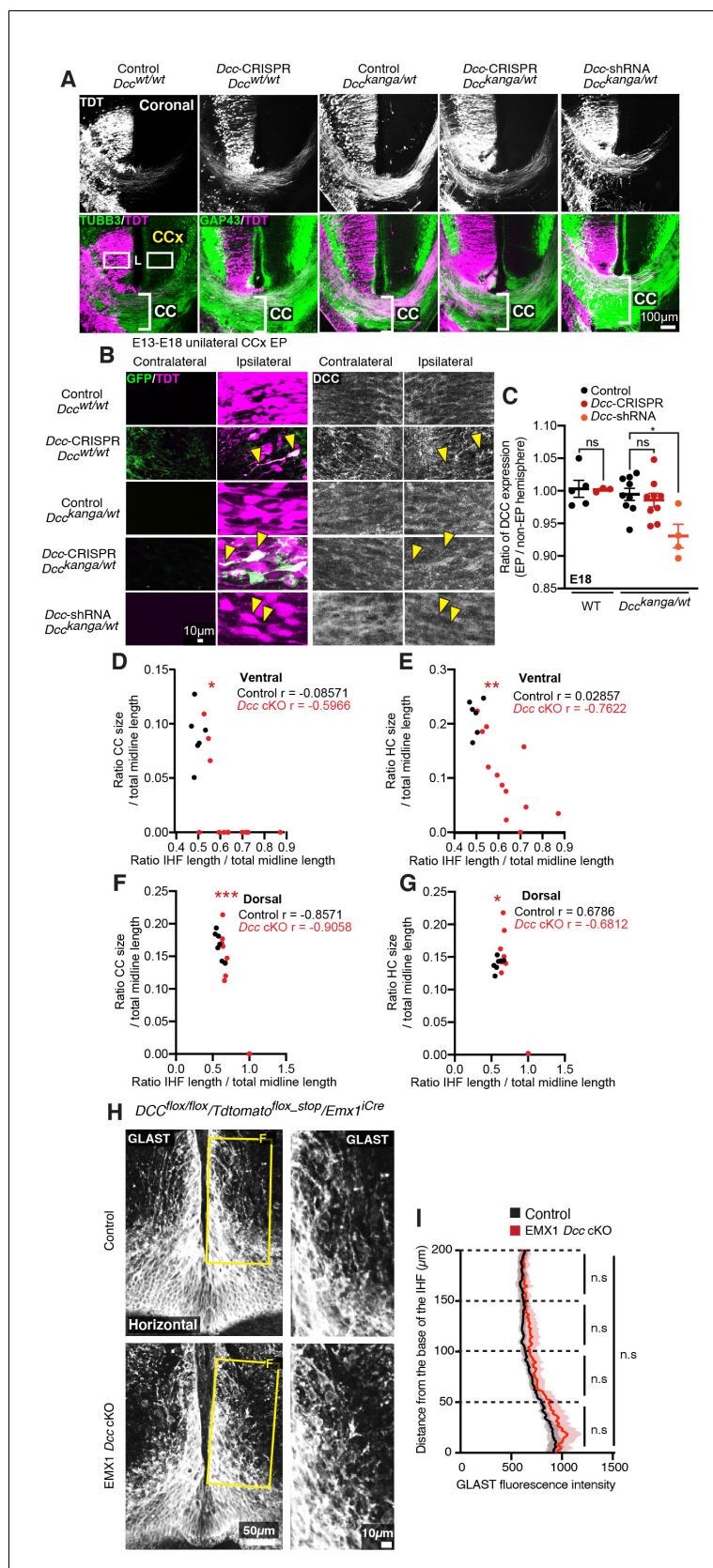


Figure 6—figure supplement 1. *Dcc* knockdown via targeted in utero electroporation does not cause corpus callosum (CC) abnormalities. (A) TUBB3 (green) and TDT (white or magenta) in E18 *Dcc*^{kanga} mice electroporated

Figure 6—figure supplement 1 continued on next page

Figure 6—figure supplement 1 continued

with pCAG-TDTOMATO and either *Dcc*-CRISPR or *Dcc*-shRNA constructs into the cingulate cortex (CCx) at embryonic day (E)13. The CC is outlined with white brackets, and white boxes indicate the location of panels represented in (B). (B) GFP (green), TDT (magenta) or deleted in colorectal carcinoma (DCC) (white) in E18 *Dcc*^{kanga} mice electroporated with pCAG-TDTOMATO and either *Dcc*-CRISPR or *Dcc*-shRNA constructs into the CCx at E13. GFP indicates expression of the *Dcc*-CRISPR, and yellow arrowheads indicate the location of select electroporated cells. (C) Quantification of the ratio of DCC expression between ipsilateral (electroporated; EP) and contralateral (non-electroporated) hemispheres shown in (B). (D–G) Scatterplots of the relationship between CC length or hippocampal commissure (HC) length normalized to total telencephalic midline length and interhemispheric fissure (IHF) length normalized to total telencephalic midline length for ventral and dorsal horizontal sections of P0 *Dcc* cKO mice. Nonparametric Spearman r correlations are shown. (H) Glial marker GLAST (white) in E15 *Dcc* cKO mice demonstrates the distribution of GLAST-positive MZG. Yellow boxes indicate region shown in insets, right and quantified in (E). (I) Quantification of mean GLAST fluorescence within the telencephalic hinge from insets in (H).

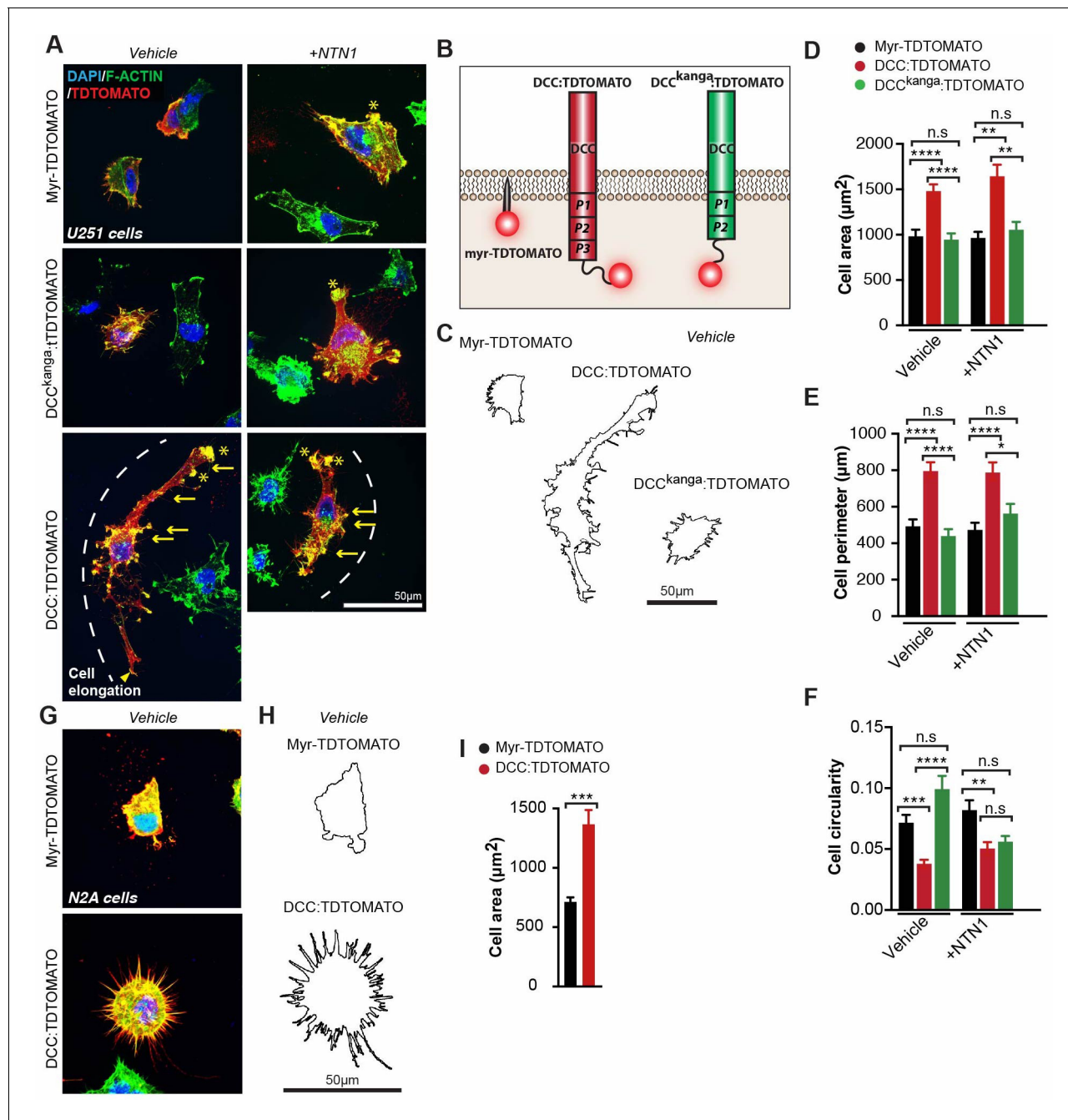


Figure 7. Netrin 1-deleted in colorectal carcinoma (NTN1-DCC) signalling promotes cytoskeletal remodelling of astroglia. (A, G) Representative images of U251 glioblastoma cells (A) and N2A cells (G) immunolabelled for TDTOMATO (red) and F-actin (green) following transfection with plasmids encoding Myr-TDTOMATO, DCC:TDOTOMATO or DCC^{kanga}:TDOTOMATO demonstrating the presence of actin-rich regions resembling filopodia (yellow arrows), lamellipodia (yellow arrowheads) and membrane ruffles (yellow asterisks) with/without stimulation with recombinant mouse NTN1 protein. (B) Schema of predicted structure of proteins on the cell membrane encoded by the plasmids expressed in cells from (A) and (G). (C, H) Outline of cell perimeter generated from images in (A) and (G), respectively. (D–F, I) Quantification of the area, perimeter and circularity of cells represented in (A) and (G). Graphs represent mean \pm SEM. Statistics by Kruskal–Wallis test for multiple comparisons. n.s.: not significant; *p<0.05, **p<0.01, ***p<0.001, ****p<0.0001. See related **Figure 6—figure supplement 1** and **Supplementary file 1**.

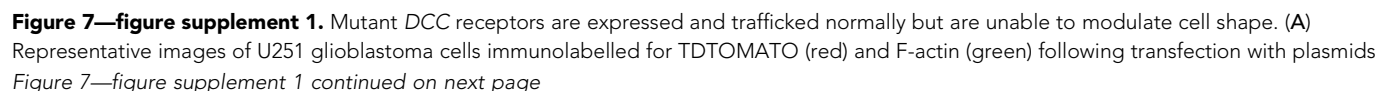


Figure 7—figure supplement 1 continued

encoding TDTOMATO, DCC:TDTOMATO or DCC^{kanga}:TDTOMATO demonstrating predominant presence or absence of colocalized TDTOMATO with F-actin (arrowheads). (B) Quantification of average cell area from U251 cells represented in (A). (C) Specific missense mutations were introduced into mouse pCAG-DCC:TDTOMATO, and exon 29 was removed (del = deleted) to create the DCC^{kanga}:TDTOMATO construct. (D) COS-7 cells were transfected with pCAG-DCC:TDTOMATO constructs, including those carrying specific point mutations and the DCC^{kanga}:TDTOMATO construct. After 48 hr, cells were lysed, and a western blot was performed for mouse deleted in colorectal carcinoma (DCC) and GADPH. Specific bands at 214 kD and 37 kD are shown. (E) HEK293T, N2A and U251 cells were transfected with pCAG-DCC:TDTOMATO constructs, including those carrying specific point mutations. After 24 hr, cells were fixed and immunohistochemistry was performed for the N-terminal of DCC without permeabilization to detect membrane-inserted DCC (HEK293T) or for the C-terminal of DCC with permeabilization (N2A and U251 cells). (F) Representative images of N2A cells immunolabelled for TDTOMATO (red) and F-actin (green) following transfection with plasmids encoding DCC:TDTOMATO carrying missense mutations and stimulated with recombinant mouse NTN1 protein with cell perimeter outlined below. The cell perimeter and cell circularity of these cells and those represented in **Figure 7B** are quantified in (G) and (H), respectively. (I) Representative images of U251 and N2A cells immunolabelled for TDTOMATO (magenta) and cleaved-caspase 3 (CC3; green) following transfection with plasmids encoding DCC:TDTOMATO and myr-TDTOMATO. Arrowheads indicate TDTOMATO-positive/CC3-positive cells, which are quantified below. (J) U251 and N2A cells were transfected with plasmids encoding myr-TDTOMATO and DCC:TDTOMATO or not transfected. After 20 hr, cells were lysed, and a western blot was performed for mouse DCC, netrin 1 (NTN1) and GADPH. Specific bands at 214 kD, 75 kD and 37 kD are shown from n = 3 biological replicates. All graphs represent mean ± SEM. Statistics by Kruskal–Wallis test for multiple comparisons. n.s.: not significant with p>0.05, *p<0.05, **p<0.01, ***p<0.001, ****p<0.0001. See related **Figure 6**, **Figure 7** and **Supplementary file 1**. All graphs represent mean ± SEM. Statistics by Mann–Whitney test or unpaired t-test: *p<0.05; n.s.: not significant with p>0.05. See related **Figure 7**, **Figure 8** and **Supplementary file 1**.

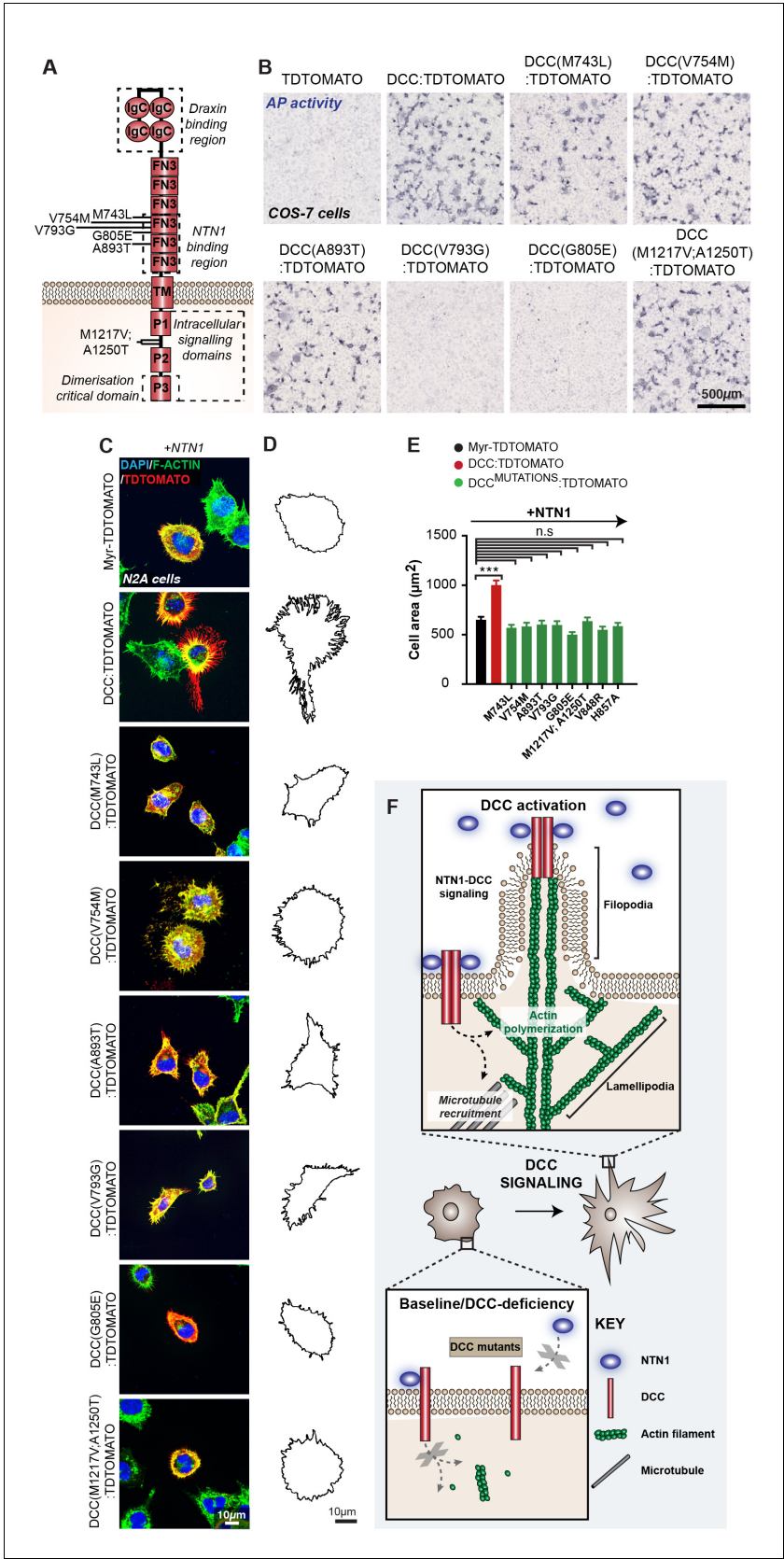


Figure 8. DCC mutations associated with human callosal agenesis are unable to modulate cell shape and show varied netrin 1 (NTN1) binding. (A) Schema of transmembrane receptor deleted in colorectal carcinoma (DCC) and its structural domains. Lines indicate the position of altered residues

Figure 8 continued on next page

Figure 8 continued

from missense *DCC* pathogenic variants identified in human individuals with corpus callosum (CC) abnormalities. FN3: fibronectin type III-like domain; IgC: immunoglobulin like type C domain; TM: transmembrane domain; p: P motif. (B) Colorimetric detection of alkaline phosphatase activity in COS-7 cells transfected with plasmids encoding TDTOMATO, DCC:TDTOMATO and mutant DCC:TDTOMATO constructs and incubated with a NTN1 alkaline phosphatase fusion protein. (C) Representative images of N2A cells immunolabelled for TDTOMATO (red) and F-actin (green) following transfection with plasmids encoding Myr-TDTOMATO, DCC:TDTOMATO or DCC:TDTOMATO carrying missense mutations and stimulated with recombinant mouse NTN1 protein. (D) Outline of cell perimeter generated from images in (B). (E) Quantification of the area of cells represented in (B). Graph represents mean \pm SEM. Statistics by Kruskal–Wallis test for multiple comparisons. n.s: not significant, *** $p < 0.001$. (F) Schema of model for DCC-mediated changes in cell shape: activation of DCC by NTN1 induces dimerization of the receptor and recruits intracellular signalling effectors to regulate actin polymerization for filopodia and lamellipodia formation, and to regulate microtubule dynamics to promote membrane protrusions. Mutations that affect DCC signalling prevent DCC-mediated changes in cell shape. See related **Figure 6—figure supplement 1** and **Supplementary file 1**.